J Eng Math (2010) 67:85–94
DOI 10.1007/s10665-009-9321-z

Limiting behaviour of particles in Taylor–Couette flow

Karen L. Henderson · D. Rhys Gwynllyw

Received: 23 December 2008 / Accepted: 3 August 2009 / Published online: 2 September 2009

Abstract Negatively buoyant inertial particles are tracked in a steady Taylor vortex background flow with gravity acting along the axis of the cylinders. Particles are found to either fall through the apparatus due to gravity or to be within retention zones. The particles within these retention zones tend towards a limit orbit in the meridional plane. It is found that for particles with density close to that of the background fluid, the size of the retention zone is relatively large with the centre of the limit orbit being close to that of the Taylor vortex. As the particle density increases, the size of the retention zone decreases and the centre of the limit orbit moves away from the centre of the Taylor vortex. The effect of varying the fluid and particle parameters on the retention zone and orbit size is investigated.

Keywords Buoyancy · Inertial particles · Settling behaviour · Taylor–Couette flow

1 Introduction

Taylor–Couette flow, in which fluid is contained between two concentric rotating cylinders, has been the subject of many experimental, analytical and numerical studies over the years [1–4]. In the case of the outer cylinder being fixed, as the rotation rate of the inner cylinder is increased the flow state goes through transitions, the first few being from laminar flow to steady axisymmetric Taylor vortices to wavy Taylor vortices.

The Couette apparatus is used as a rotating filter for many purposes [5–7]. Specific applications include separating plasma from blood [8], a photocatalytic reactor for water purification [9] and a bioreactor for the culture of animal cells [10]. A recent review of its applications has been written by Vedantam and Joshi [11].

In this paper we compute the paths of small inertial particles in a background flow of steady axisymmetric Taylor vortices using a form of the particle tracking equations established by Maxey and Riley [12]. These equations and variations thereof have been used widely for tracking particles in many different background flows; see [13] for an overview. Much of the work in the Taylor–Couette geometry [5–7] has concentrated on the filtration performance of the Couette apparatus as a filtration device as opposed to considering the motion of individual particles.

Rudman et al. [14,15] tracked inertial particles in both wavy and non-wavy vortex flow fields. The focus of their research was the strain history that inertial particles experienced due to their paths and the dispersion of fluid

K. L. Henderson (✉) · D. Rh. Gwynllyw
Department of Mathematics & Statistics, University of the West of England, Bristol, BS16 1QY, UK
e-mail: karen.henderson@uwe.ac.uk

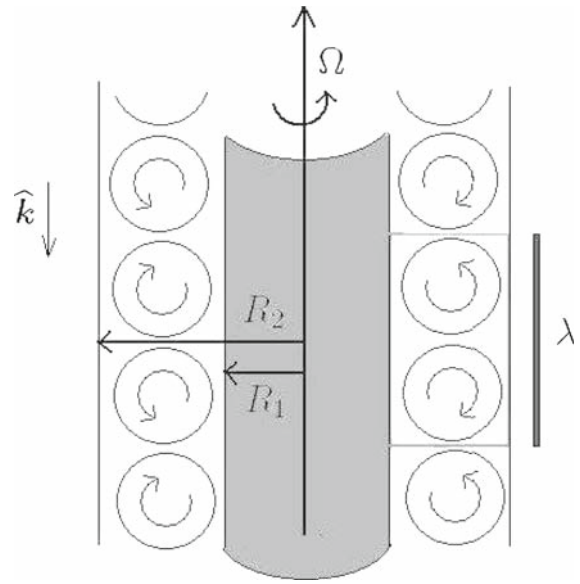

Fig. 1 Schematic of the background flow. A pair of Taylor vortices, with wavelength $\lambda \approx 2$ has been highlighted

particles as opposed to the limiting behaviour of the particles. Wereley and Lueptow [16] simulated the motion of inertial particles in Taylor–Couette flow using Davey's [17] analytical representation of the background flow. This limited the range of Reynolds numbers that could be considered. They were primarily interested in the application of a rotating filter for water purification in outer-space and therefore mostly considered particles under zero gravity. Various particle densities were considered and a net radial flow was imposed. They found that, when the buoyancy force is neglected, all particles approach a limit-cycle orbit around the central region of each Taylor vortex cell.

In previous work, Henderson et al. [18] investigated the effect the individual forces acting on the particle had on its subsequent motion. A parameter range in which the buoyancy force could be neglected was considered and hence the particle motion was isolated to a single Taylor cell. The long-term behaviour of the particles was studied together with the approach to its limiting path as the particle density and Reynolds number of the background flow were varied. In this work we extend the parameter range previously considered to investigate the limiting behaviour of particles in Taylor–Couette flow when buoyancy is taken into account.

2 Model

The background flow, computed prior to running the particle tracking code, is steady axisymmetric Taylor vortex flow as illustrated schematically in Fig. 1. The parameters for the background flow are the radius ratio $\eta = R_1/R_2$ and the Reynolds number of the inner cylinder $\mathrm{Re} = \Omega R_1 \delta/\nu$, where R_1 and R_2 are the radii of the inner and outer cylinders respectively, $\delta = R_2 - R_1$ is the gap between the cylinders, Ω is the angular velocity of the inner cylinder and ν is the kinematic viscosity of the fluid. Note that the outer cylinder is held stationary.

The numerical method used to compute the steady axisymmetric Taylor vortex background flow is based on a spectral-collocation scheme [19]. This reference gives details of the accuracy of the scheme. Note that gravity does not enter into the solution of the fluid flow but the Taylor–Couette apparatus is aligned so that the centre of the cylinders is in the direction of gravity. In this scheme we time-step the Navier–Stokes equations forward until a steady-state solution is reached; at this stage the spectral coefficients are stored. The spectral coefficients may be used to accurately compute components of the background flow at any position (r, z) in the annulus. Throughout this paper we have used spectral-collocation discretisation parameters 7 and 19 in the axial and radial directions, respectively.

The motion of the inertial particles is tracked using a form of the equation taken from Maxey and Riley [12] with the corrected form for the added mass force, as detailed by Auton et al. [20]. The particles are assumed to be spherical with radius a_p and to be inertial, that is, the particles do not affect the background flow and do not interact with one another. The equations are nondimensionalised by taking the characteristic length and velocity scales to be δ and ΩR_1 respectively. The result is the following differential equation for $\boldsymbol{u}_p$, the velocity of a particle,

$$\beta \frac{\mathrm{d}\boldsymbol{u}_p}{\mathrm{d}t} = \frac{\mathrm{D}\boldsymbol{v}_f}{\mathrm{D}t} - \tfrac{1}{2}\left\{\frac{\mathrm{d}\boldsymbol{u}_p}{\mathrm{d}t} - \frac{\mathrm{D}\boldsymbol{v}_f}{\mathrm{D}t}\right\} + \frac{1}{(\mathrm{Fr})^2}(\beta - 1)\widehat{\boldsymbol{k}} - \frac{18\alpha_p^2}{\mathrm{Re}}(\boldsymbol{u}_p - \boldsymbol{v}_f) = \boldsymbol{H}, \tag{1}$$

where $\boldsymbol{v}_f$ is the fluid's velocity at the particle's position; β, the density ratio, is the ratio of the particle density to the fluid density; $\alpha_p = 2a_p/\delta$, the particle size ratio, measures the number of particles that would fit tightly across the radial gap; $\widehat{\boldsymbol{k}}$, the unit vector denoting the direction of the gravitational force, is taken to be parallel to the axis of the cylinders. The nondimensional parameter Fr, where

$$\mathrm{Fr} = \frac{\nu \mathrm{Re}}{\sqrt{g\delta^3}}, \tag{2}$$

is the Froude number which represents the ratio of inertial to gravitational forces, and g is the magnitude of the acceleration due to gravity. In Eq. 1 the terms on the right-hand side represent the inertial force (due to the acceleration of the fluid), the added-mass force (which relates to the necessity of moving a mass of fluid displaced by the particle), the buoyancy term and the Stokes drag force (due to the viscosity of the fluid). Note that in (1) we do not include the Basset and Saffman forces nor the Faxen corrections as detailed by Mei [21]. Previously [18] we found that the combined effect of including these terms in the particle tracking equations had a significant quantitative effect on the limit cycles found for certain parameter ranges. However, in this paper, for ease of computation, we consider only the forces shown in (1). We anticipate that the results that we obtain from their neglect will be qualitatively similar to those achieved with these terms included.

Equation 1 may be rearranged, in order to make $\frac{\mathrm{d}\boldsymbol{u}_p}{\mathrm{d}t}$ the subject, as

$$\frac{\mathrm{d}\boldsymbol{u}_p}{\mathrm{d}t} = \gamma^{-1}\left(\boldsymbol{H} + \tfrac{1}{2}\frac{\mathrm{d}\boldsymbol{u}_p}{\mathrm{d}t}\right), \tag{3}$$

where $\gamma = \beta + \frac{1}{2}$. This equation needs to be solved together with the differential equation

$$\frac{\mathrm{d}\boldsymbol{r}_p}{\mathrm{d}t} = \boldsymbol{u}_p, \tag{4}$$

and initial conditions

$$\boldsymbol{r}_p(0) = \boldsymbol{r}_p^o, \quad \boldsymbol{u}_p(0) = \boldsymbol{u}_p^o, \tag{5}$$

where $\boldsymbol{r}_p(t)$ is the position of the particle at time t. Equations 3–5, which determine the particle path, are solved numerically using an implicit two-stage Runge–Kutta scheme with fixed-point iteration. A time-step of $\delta t = 4\times10^{-5}$ was sufficient in order to produce results accurate to at least graphical tolerance.

In previous work [18], where the buoyancy force was neglected, we took the initial velocity of a particle, $\boldsymbol{u}_p^o$, to be the same as the fluid velocity at $\boldsymbol{r}_p^o$. In this paper, however, we obtain $\boldsymbol{u}_p^o$ by solving Eq. 3 whilst keeping the particle's position fixed. This approach eliminates any occurrence of a sharp jump in the particle's start-up motion in the case of particle paths differing significantly from fluid-element paths [22].

Although our code is designed to account for particles colliding with the cylinder walls, few of our calculations result in such events occurring. In cases where collisions with the walls do occur, the collisions are assumed to be perfectly elastic.

3 Results

For all the results presented in this paper we consider a radius ratio of $\eta = 0.75$ to compute the background flow. The advantage of choosing this particular value is that the Taylor-vortices regime is stable for a relatively wide

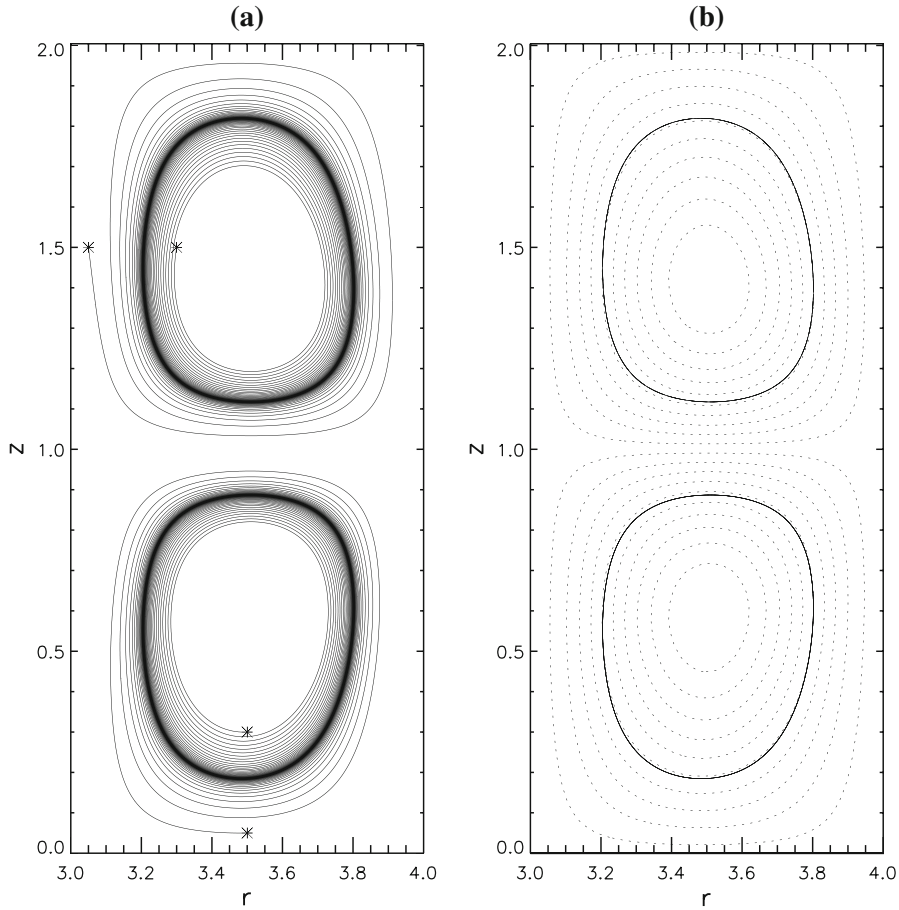

Fig. 2 Neglecting the buoyancy term (Fr $\to \infty$). **a** Paths of four particles ($\beta = 5, \alpha_p = 30$), whose initial positions are denoted by *stars*, in a background flow with Reynolds number Re $= 130$. **b** *Dotted*: contour plots of the stream function of the background flow. *Solid*: limit cycles, in the meridional plane, of the particles shown in (**a**)

range of Reynolds numbers [2,23], that is the onset of wavy Taylor vortices occurs at values of Re much higher than $\mathrm{Re}^* = 85.8$, the critical Reynolds number at which Couette flow becomes unstable.

All plots are over a period λ of the background flow; see Fig. 1, which contains a pair of Taylor cells. The rotating inner cylinder forms the left vertical boundary and the stationary outer cylinder forms the right-hand vertical boundary. The chosen period is such that the top Taylor cell rotates counter-clockwise with the bottom Taylor cell rotating clockwise.

In Fig. 2 we illustrate the behaviour of particles when the buoyancy term is neglected (Fr $\to \infty$). Similar results have been presented in [16,18]. The consequence of neglecting the buoyancy term is that particles starting within a Taylor cell remain in that Taylor cell. In Fig. 2a we plot the projection in the meridional plane of the paths of four particles ($\beta = 5, \alpha_p = 30$) with different initial positions in a background flow with Re $= 130$. The paths can be considered to be a superposition of azimuthal motion about the inner cylinder and toroidal motion in the vertical plane. For a given Taylor cell, all particles starting within the cell tend towards a limit cycle in the meridional plane, contained within that cell. A pair of Taylor cells is shown in Fig. 2a and within each cell there are two particles, whose initial positions are inside and outside of their associated limit cycle. The figure displays the motion of these particles towards their limit cycle, which is contained in the darker region of Fig. 2a and plotted in Fig. 2b by a solid line. Wereley and Lueptow [16] considered the radial component of the forces acting on particles inside, on and outside the limit orbit. They concluded that it was the relative balance of the inertial and drag forces that determined

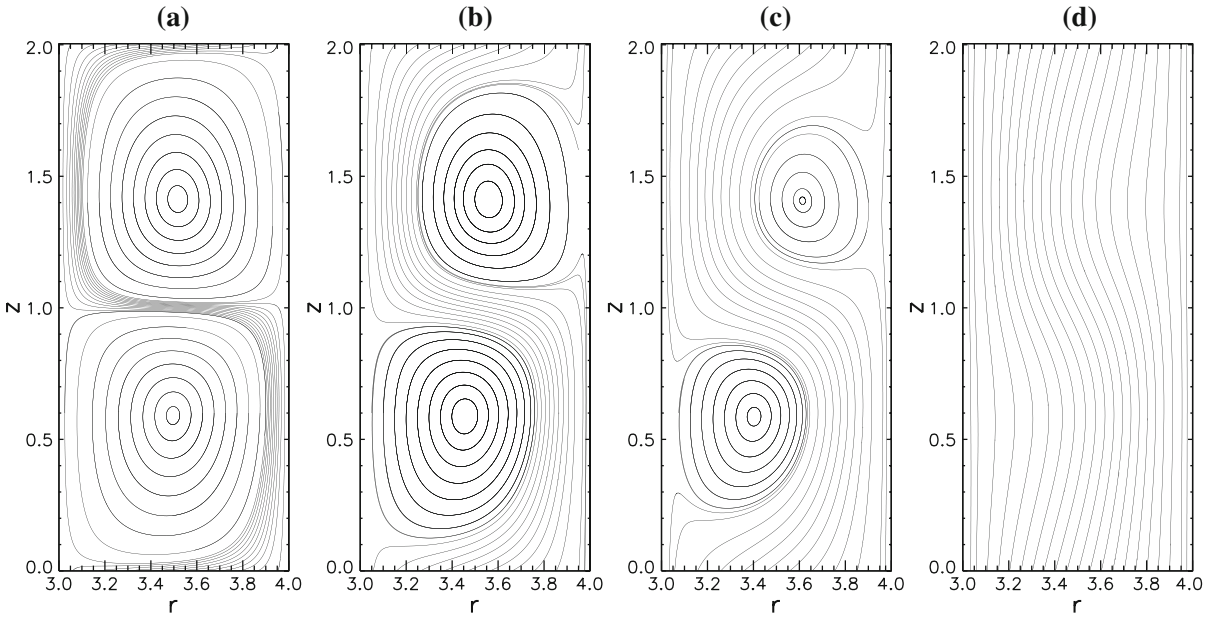

Fig. 3 The paths of several particles ($\alpha_p = 30$) with **a** $\beta = 1.01$, **b** $\beta = 1.05$, **c** $\beta = 1.1$, **d** $\beta = 1.5$, in a flow of Re = 130. Gravity is acting downwards

the position of the particle relative to its original radial position near the inner cylinder after each revolution. Figure 2b displays the limit cycles against contours of the stream function, which correspond to fluid-element paths. As reported previously [16,18] we observe that the limit cycles are different to the fluid-element paths.

The darker banded region in Fig. 2a is due to the progressively slower rate that the particles (from both inside and outside the limit cycle) approach their limit cycle. A relatively large value of β has been used here to better illustrate the features of the particle paths; a similar qualitative behaviour is observed for all $\beta > 1$ [16,18]. The effect of changing β on the approach to the limit cycle has been considered in detail in previous work [18] and, using lower values of β, results in a slower rate of approach to the limit orbit. Thus, if a physically realistic value of β had been used for Fig. 2, the banded region would been more pronounced which would have visually masked the individual particle paths to an even greater extent.

Our key aim in this paper is to better understand the behaviour of particles when the buoyancy term is taken into account, through Eq. 1. In particular we want to examine the effect of varying the particle parameters (β, α_p) and the flow parameters (Re, Fr) on the limiting behaviour of the particles.

In Fig. 3 we illustrate the behaviour of the particles when gravity is taken into account. This is taken to act downwards, parallel to the axis of the cylinders. The stream function for the background flow is as in Fig. 2b. The value of $\mathrm{Fr} = 1 \times 10^{-3}\mathrm{Re}$ is used in this and all subsequent figures except for Fig. 8. All particles have $\alpha_p = 30$ and are in a background flow with Re = 130. The density ratios are taken to be $\beta = 1.01, 1.05, 1.1, 1.5$ in Fig. 3a–d, respectively.

For density ratios close to unity (Fig. 3a) we find that particles which are initially in the inflow, at the top of the Taylor vortex pair ($z = 2\pi/\alpha \approx 2$) wind around the Taylor vortices, falling close to the inner cylinder in the counter-clockwise (top) cell and close to the outer cylinder in the clockwise (bottom) cell. We only plot a pair of Taylor cells here, but because the background flow is periodic with period λ this winding behaviour would continue as the particles fall through the apparatus. Not all particles fall through the apparatus. Some get caught in a cycling motion and the region containing such particles is referred to as the retention zone [14]. Within both retention zones of Fig. 3a the particle paths have been plotted over a small number of periods. What is not clear from the figure is that, given a particular retention zone, all the cycling particles tend towards a unique limit cycle. Had we continued the particle tracking of Fig. 3a over a longer period of time then the retention zone would contain a large dark region

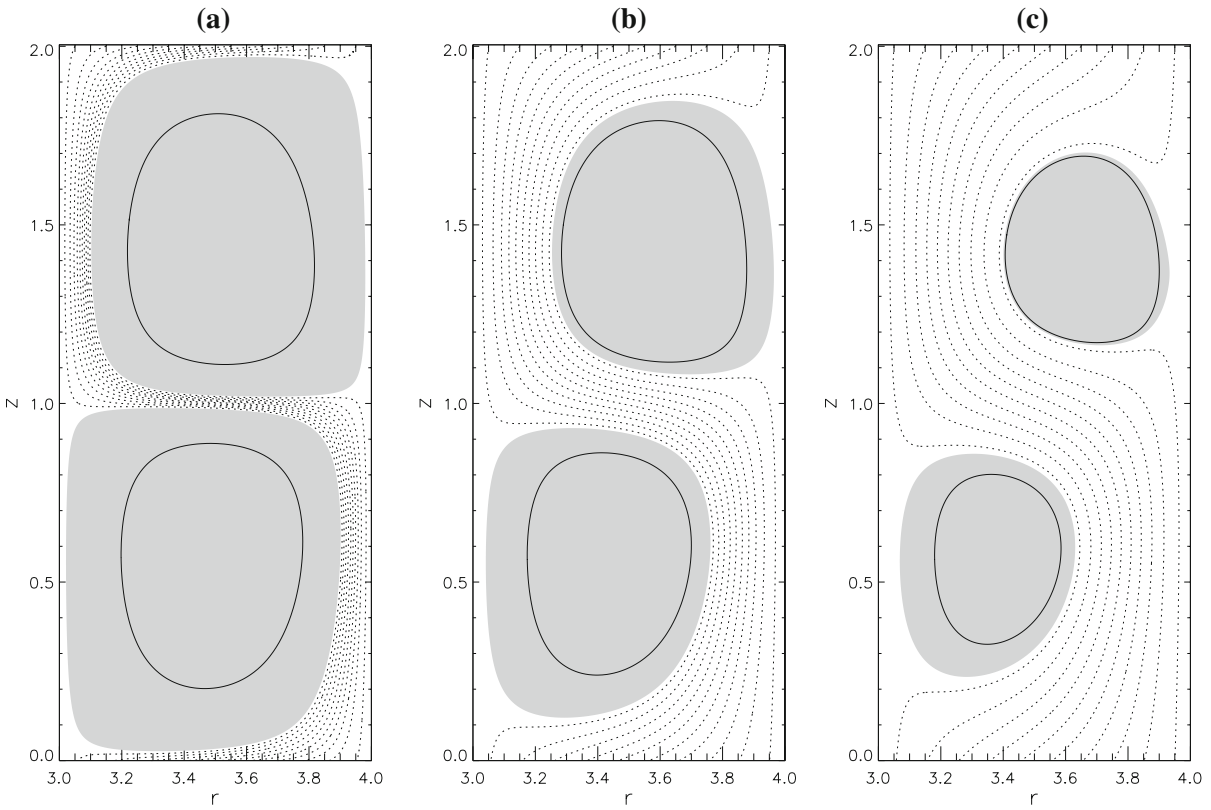

Fig. 4 **a** $\beta = 1.01$, **b** $\beta = 1.05$, **c** $\beta = 1.1$. *Solid lines*: limit cycles; *dotted lines*: the paths of several particles which fall through the Taylor cells. The shaded areas represent the retention zones. Flow/particle parameters: $\alpha_p = 30$, Re $= 130$

due to the banding effect described earlier, related to Fig. 2a. Hence, within the retention zones of Fig. 3a, some of the particles are slowly moving inwards towards the limit cycle whilst some are moving outwards towards the same limit cycle.

With higher density ratios such as $\beta = 1.05$ and $\beta = 1.1$ (Fig. 3b, c) a greater proportion of the particles follow the winding motion and hence will fall through the Taylor cells. For both these cases retention zones still exist, but their size is reduced as β is increased. In addition, the retention zones are offset, that is, the centre of the retention zone in the counter-clockwise Taylor cell is closer to the outer cylinder and the centre of the retention zone of the clockwise Taylor cell is closer to the inner cylinder. This effect is more pronounced as β is increased.

For even higher density ratios such as $\beta = 1.5$ (Fig. 3d) retention zones no longer exist and all particles fall through the cells. Similar qualitative results have been presented by Rudman [14] and Wereley and Lueptow [16].

In Fig. 4 we plot the retention zones (shaded) and limit cycles (solid lines) corresponding to Fig. 3a–c. The dashed lines correspond to particles paths of some falling particles.

Both the limit cycles and subsequent retention zones are calculated using a bisection method approach. The limit cycle is the line that partitions particles that spiral outwards towards the limit cycle from those that spiral inwards, or fall through the Taylor cell. The limit cycle obtained by the bisection method approach has been verified by starting with two particles (one spiraling inwards and the other outwards) and running the particle tracking code until the two particles have reached the limit cycle. The retention zone is the region that partitions particles that spiral inwards towards the limit cycle from those that fall through the Taylor cell. We note that falling (winding) particles may get attracted into retention zones of Taylor cells below the one in which they start. This occurs for a small number of particles that start on particle paths that pass close to the retention zone. For finite aspect ratio

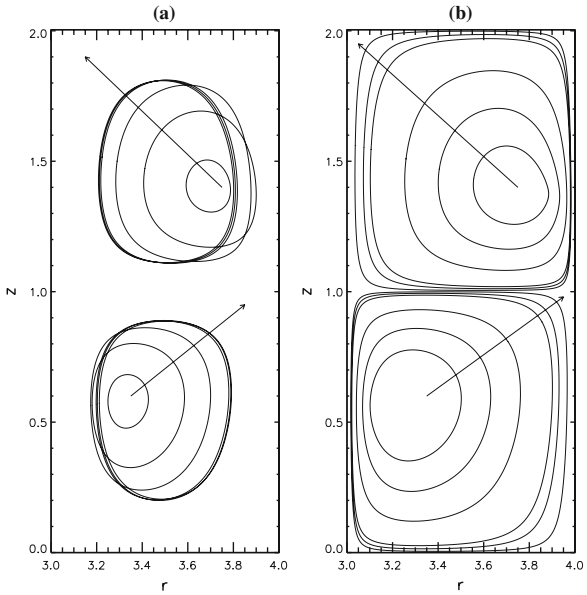

Fig. 5 **a** Limit cycles and **b** Retention zones for $\beta = 1.001$, 1.005, 1.01, 1.05, 1.1, 1.15. The *arrows* show the direction of decreasing β. Flow/particle parameters: $\alpha_p = 30$, Re $= 130$

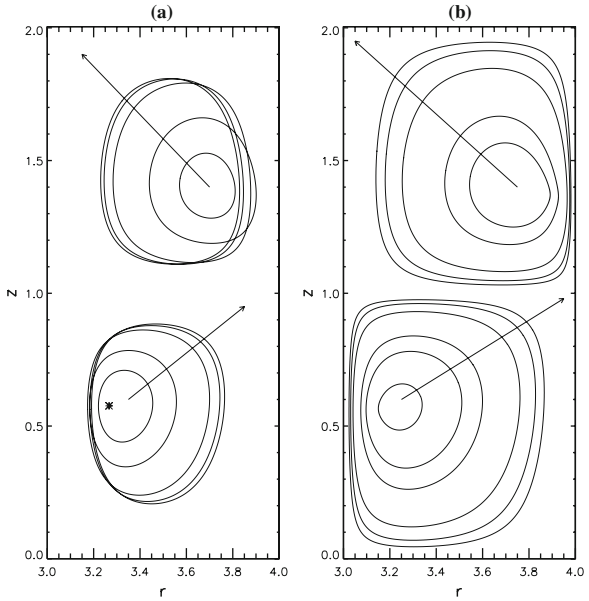

Fig. 6 **a** Limit cycles and **b** retention zones for $\alpha_p = 15$, 17.5, 20, 30, 40, 50. The *arrows* show the direction of increasing α_p. Note that for $\alpha_p = 15$ there is a limit point in the clockwise cell, illustrated by a *star*, but no limit point exists in the counter-clockwise cell. Flow/particle parameters: $\beta = 1.05$, Re $= 130$

apparatus, this would mean that the limit orbits in the cells at the bottom of the apparatus would contain slightly more particles than those at the top.

All particles within a retention zone will remain in that retention zone and tend to the corresponding limit cycle. From Fig. 4 we can see that both the limit cycles and their associated retention zones decrease in size as β is increased and become more offset. In addition, there is a difference between the retention zones and limit cycles corresponding to the two Taylor cells, which is most pronounced as β increases. In this case, the limit cycle for the clockwise cell is smaller than that of the counter-clockwise cell and the limit cycle in the top cell is much closer to the edge of the retention zone than in the lower cell.

In Fig. 5 we plot the limit cycles and retention zones for various values of $\beta > 1$ for particles with $\alpha_p = 30$ and background flow of Re $= 130$. We can see that as the density ratio increases the size of both the limit orbits and the retention zones decreases, hence the proportion of particles attracted to these limit orbits also decreases. In addition as β increases we find that the centres of both the limit cycles and retention zones move from the centre of the Taylor cell. In the clockwise Taylor cell, increasing β results in the limit cycle and retention zone moving towards the inner cylinder. In the counter-clockwise Taylor cell the opposite is the case. Further, in terms of the size of both the limit cycle and retention zone, the differences between the clockwise and counter-clockwise Taylor cells are more pronounced as β increases.

For values of β close to unity, the buoyancy term in (1) becomes less important. As a result, the resulting limit cycles are very close to each other and to that obtained when buoyancy is neglected [18]. As expected, as the values of β approach unity, the retention zones approach the full Taylor cell.

In Fig. 6 we plot the limit cycles and retention zones for various values of α_p for particles with $\beta = 1.05$ and flow Re $= 130$. We can see that as the particle size ratio increases, the size of both the limit orbits and the retention zones decrease and their centres move away from the centre of the Taylor cell, as for the case of increasing β. For the particular case of $\alpha_p = 15$ we find a limit point, as opposed to a limit cycle in the clockwise Taylor cell, illustrated

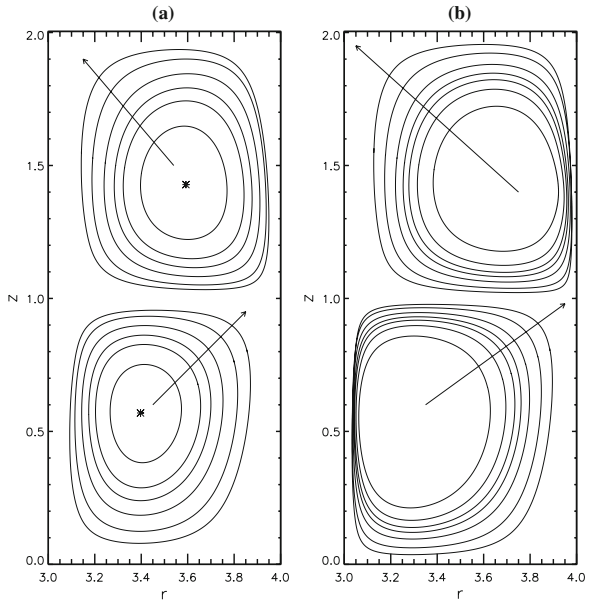

Fig. 7 **a** Limit cycles and **b** retention zones for Re = 100, 110, 120, 130, 150, 200, 300. The *arrows* show the direction of increasing Re. Limit points are found for Re = 100 and illustrated by a *star*. Particle parameters: $\beta = 1.05$, $\alpha_p = 30$

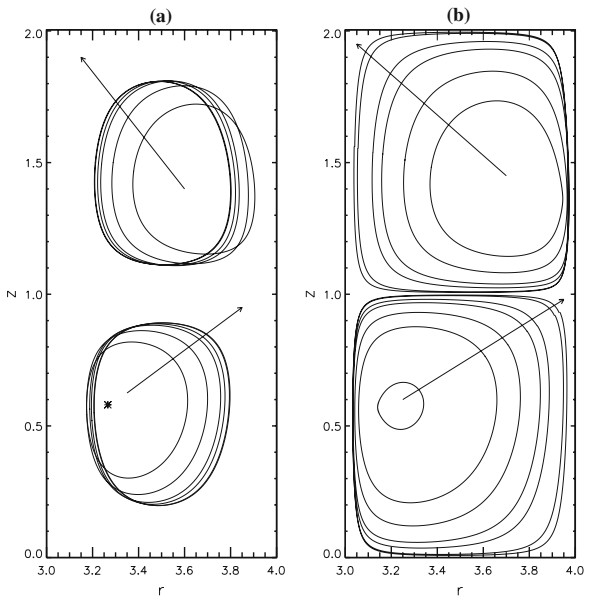

Fig. 8 **a** Limit cycles and **b** retention zones for Fr/Re = 7.5×10^{-4}, 1×10^{-3}, 1.5×10^{-3}, 2×10^{-3}, 5×10^{-3}, 1×10^{-2}. The *arrows* show the direction of increasing Fr/Re. A limit point is found for Fr/Re = 5×10^{-4} in the clockwise cell only and this is illustrated by a *star*. Flow/particle parameters: Re = 130, $\beta = 1.05$, $\alpha_p = 30$

in Fig. 6a by a star, and all particles within the corresponding retention zone will spiral towards this point. No limit point/cycle was found in the counter-clockwise cell and therefore no retention zone exists for $\alpha_p = 15$ in this cell. In the case that no limit point/cycle exists we find that all particles will eventually fall through the cell leaving a void. Depending on the particle's initial position this can occur either immediately or after the particle follows an outwardly spiralling path for a number of revolutions.

In Fig. 7 we plot the limit cycles and retention zones for various values of Re for particles with $\beta = 1.05$ and $\alpha_p = 30$. We find that the limit cycles increase in size as the Reynolds number is increased. This was also observed in the zero gravity case [18]. For Re = 100 we find a limit point as opposed to a limit orbit. Note that for this case the retention zone is quite large and we find that as the Reynolds number is reduced further, a limit point persists but that the retention zone shrinks in size. For the flow parameters shown here, the critical Reynolds number at which vortices disappear is Re = 85.8.

In Fig. 8 we plot the limit cycles and retention zones for various values of Fr/Re for particles with $\beta = 1.05$ and $\alpha_p = 30$ in a flow with Re = 130. We find that the effect of increasing Fr/Re is qualitatively similar to increasing both β and α_p. Note that for Fr/Re = 5×10^{-4} there are no limit cycles but a limit point is found in the bottom Taylor cell only. The limit cycles for Fr/Re = 5×10^{-3} and Fr/Re = 1×10^{-2} are indistinguishable from each other and correspond to the limit orbits found when buoyancy effects are neglected.

4 Conclusion

We have computed the path of negatively buoyant particles in a Taylor vortex for cases when the buoyancy term in the particle tracking equations may not be neglected. Our results are interesting in that we find that for certain parameter regimes particles follow paths which tend to limit orbits which are very different to fluid-element paths.

This shows that care needs to be exercised in choosing tracer particles depending on what flow properties are to be visualised. Particles with high density ratio fall through the cells but as the density ratio is reduced we find that retention zones exist. Particles within these zones tend to a limit cycle or limit point in the meridional plane, whilst those particles which are not in these retention zones fall through the Taylor cells. For particles with density close to that of the fluid, this fall occurs in a winding motion about the Taylor vortices.

The key aim of this paper was to consider the effect of varying the particle parameters β and α_p and the flow parameters Re and Fr on the nature of the limit cycles and associated retention zones. We find that the limit cycles and retention zones reduce in size as the density ratio is increased and also for decreasing particle size ratio. A similar behaviour is seen for increasing Re and decreasing Fr/Re. In addition, for the cases when β is increased, α_p is decreased and Fr/Re is decreased, the centres of the limit cycles move away from the centre of the Taylor cells; being closer to the outer cylinder wall in the counter-clockwise Taylor cell and closer to the inner cylinder wall in the clockwise Taylor cell. Differences in the size and shape of the two limit cycles in each pair of Taylor cells occur and in some cases we find a retention zone in the clockwise Taylor cell only.

Kawai et al. [24] recently set up an experiment to visualise for the first time the limit orbits predicted numerically [16,18]. They used a small aspect ratio Couette apparatus and were able to visualise limit orbits under certain conditions. Our results will hopefully provide the motivation for further experiments in this area and give an indication as to parameter regimes in which limit orbits may be found.

Acknowledgements Both authors of this paper gratefully acknowledge the privilege of having worked with Howell Peregrine. Both KLH and DRhG obtained their PhDs from the Department of Mathematics at Bristol University. KLH was a postdoctoral research assistant to Howell from 1994 to 1995 and Howell was DRhG's supervisor for his PhD studies from 1988 to 1991. Howell's enthusiasm and knowledge of Applied Mathematics was inspirational to both of us. His introductory lecture to doctoral students in 1988 remains in our memory and included a video demonstrating the classical Taylor–Couette experiment.

References

1. Taylor GI (1923) Stability of a viscous liquid contained between two rotating cylinders. Phil Trans R Soc Lond A 223:289–343
2. Davey A, Di Prima RC, Stuart JT (1968) On the instability of Taylor vortices. J Fluid Mech 31:17–52
3. Jones CA (1981) Nonlinear Taylor vortices and their stability. J Fluid Mech 102:249–261
4. Fenstermacher PR, Swinney HL, Gollub JP (1979) Dynamical instabilities and the transition to chaotic Taylor vortex flow. J Fluid Mech 94:103–128
5. Lueptow RM (1995) Fluid mechanics of a rotating filter separator. In: Choi KJ (ed) Advances in filtration and separation technology, vol 9. American Filtration and Separations Society, pp 283–291
6. Holeschovsky UB, Cooney CL (1991) Quantitative description of a ultrafiltration in a rotating filtration device. AIChE J 37: 1219–1226
7. Belfort G, Mikulasek P, Pimbley JM, Chung KY (1993) Diagnosis of membrane fouling using a rotating annular filter. 2. Dilute particle suspensions of known particle-size. J Memb Sci 77:23–39
8. Ohashi K, Tashiro K, Kushiya F, Matsumoto T, Yoshida S, Endo M, Horio T, Ozawa K, Sakai K (1988) Rotation-induced Taylor vortex enhances filtrate flux in plasma separation. Trans Am Soc Artif Intern Organs 34:300–307
9. Dutta PK, Ray AK (2004) Experimental investigation of Taylor vortex photocatalytic reactor for water purification. Chem Eng Sci 59:5249–5259
10. Haut B, Ben Amor H, Coulon L, Jacquet A, Halloin V (2003) Hydrodynamics and mass transfer in a Couette-Taylor bioreactor for the culture of animal cells. Chem Eng Sci 58:777–784
11. Vedantam S, Joshi JB (2006) Annular centrifugal contractors—a review. Chem Eng Res Des 84:522–542
12. Maxey MR, Riley JJ (1983) Equation of motion for a small rigid sphere in a nonuniform flow. Phys Fluids 26:883–889
13. Michaelides EE (1997) Review—the transient equation of motion for particles, bubbles and droplets. J Fluids Eng 119:233–247
14. Rudman M, Thompson MC, Hourigan K (1994) Particle shear-rate history in a Taylor-Couette column. Liquid-solid flows. ASME 189:23–30
15. Rudman M (1998) Mixing and particle dispersion in the wavy vortex regime of Taylor-Couette flow. AIChE J 44:1015–1026
16. Wereley ST, Lueptow RM (1999) Velocity field for Taylor-Couette flow with an axial flow. Phys Fluids 11:325–333
17. Davey A (1962) The growth of Taylor vortices in flow between rotating cylinders. J Fluid Mech 14:336–368
18. Henderson KL, Gwynllyw DRh, Barenghi CF (2007) Particle tracking in Taylor Couette flow. Eur J Mech B Fluids 26:738–748
19. Henderson KL, Barenghi CF (1995) Numerical methods for helium's two fluid model. J Low Temp Phys 98:351–381
20. Auton TR, Hunt JCR, Prud'homme M (1988) The force exerted on a body in inviscid unsteady non-uniform rotational flow. J Fluid Mech 197:241–257

21. Mei RW (1994) Flow due to an oscillating sphere and an expression for unsteady drag on the sphere at finite Reynolds number. J Fluid Mech 270:133–174
22. Gwynllyw DRh, Phillips TN (2005) Some issues regarding spectral element meshes for moving journal bearing system. Int J Numer Methods Fluids 48:423–454
23. Jones CA (1985) The transition to wavy Taylor vortices. J Fluid Mech 157:135–162
24. Kawai H, Kudo H, Takahashi H (2007) Visualization of a limit cycle orbit in a Taylor vortex flow with a short annulus. J Chem Eng Jpn 40:944–950